Simulation of keratoconus observation in photorefraction

Ying-Ling Chen[1], B. Tan[1], K. Baker[1], and J. W. L. Lewis[1]

[1]Center for Laser Applications, The University of Tennessee Space Institute, 411 B. H. Goethert Parkway, Tullahoma, Tennessee 37388-8897
ychen@utsi.edu, jlewis@utsi.edu

T. Swartz[2], Y. Jiang[2], and M. Wang[2,3]

[2] Wang Vision Institute, Nashville, &
[3]Department of Ophthalmology, University of Tennessee, Memphis, TN

Abstract: In the recent years, keratoconus (KC) has increasingly gained attention due to its treatment options and to the popularity of keratorefractive surgery. This paper investigates the potential of identification of KC using photorefraction (PR), an optical technique that is similar to objective retinoscopy and is commonly used for large-scale ocular screening. Using personalized eye models of both KC and pre-LASIK patients, computer simulations were performed to achieve visualization of this ophthalmic measurement. The simulations are validated by comparing results to two sets of experimental measurements. These PR images show distinguishable differences between KC eyes and eyes that are either normal or ametropic. The simulation technique with personalized modeling can be extended to other ophthalmic instrument developments. It makes possible investigation with the least number of real human subjects. The application is also of great interest in medical training.

OCIS codes: (330.4060) Modeling of vision; (330.4460) Ophthalmic optics; (170.4580) Optical diagnostics for medicine; (170.4460) Ophthalmic optics

References and links

1. E. H. Roth, H. Ludwig, F. Schmitz, and W. Werner, "Retinoscopy. A multi-media teaching program on CD," Ophthalmologe. **98**, 964-967 (2001).
2. I. Chopra, and A. K. Jain, "Between eye asymmetry in keratoconus in an Indian population," Clin. Exp. Optom. **88**, 146-152 (2005).
3. J. Kim, and M. V. Netto, "Keratoconus associated with hyperimmunoglobulin E syndrome," Cornea. **23**, 93-96 (2004).
4. H. Howland, "Optics of photoretinoscopy: results from ray tracing," Am. J. Optom. Physiol. Opt. **62**, 621-625 (1985).
5. W. Bobier, "Eccentric photorefraction: Optical analysis and empirical measures," Am. J. Optom. Physiol. Opt. **62**, 614-620 (1985).
6. R. Navarro, L. Gonzalez, and J. L. Hernandez-Matamoros, "On the prediction of optical aberrations by personalized eye models," Optom. Vis. Sci. **83**, 371-381 (2006).
7. C. Winkler von Mohrenfels, A. Huber, B. Gabler, W. Herrmann, A. Kempe, C. Donitzky, and C. .P. Lohmann, "Wavefront-guided laser epithelial keratomileusis with the wavelight concept system 500," J. Refract. Surg. **20**, S565-569 (2004).
8. J. Castanera, A. Serra, and C. Rios, "Wavefront-guided ablation with Bausch and Lomb Zyoptix for retreatments after laser in situ keratomileusis for myopia," J. Refract. Surg. **20,** 439-443 (2004).
9. D. Y. Lin, and E. E. Manche, "Custom-contoured ablation pattern method for the treatment of decentered laser ablations. J. Cataract Refract. Surg. **30,** 1675-1684 (2004).
10. J. B. Almeida, and A. M. Garcia, "Theoretical calculation of a contact lens thickness designed to correct the eye's monochromatic aberrations," Optom. Vis. Sci. **82,** 59-63 (2005).

#74906 - $15.00 USD Received 11 September 2006; revised 26 October 2006; accepted 30 October 2006

11. J. Marsack, T. Milner, G. Rylander, N. Leach, and A. Roorda, "Applying wavefront sensors and corneal topography to keratoconus," Biomed. Sci. Instrum. **38**, 471-476 (2002).
12. W. N. Charman, "Wavefront technology: past, present and future," Cont. Lens Anterior Eye **28**, 75-92. Epub 2005 Apr 26. Review (2005).
13. R. Navarro, J. Santamaria, and J. Bescos, "Accommodation-dependent model of the human eye with aspherics," J. Opt. Soc. Am. A **2**, 1273-1281 (1985).
14. T. O. Salmon, and C. van de Pol, "Zernike coefficient norms – comparison of studies," presented at the American Academy of Optometry annual meeting, Tampa, Florida, 9 December, 2004.
15. I. J. Hodgkinson, K. M. Chong, and A. C. B. Molteno, "Photorefraction of the living eye: a model for linear knife edge photoscreening," Appl. Opt. **30**, 2263-2269 (1991).
16. J. J. Weiter, F. C. Delori, G. L. Wing, and K. A. Fitch, "Retinal pigment epithelium lipofuscin and melanin and choroidal melanin in human eyes," Invest. Opthalmol. Vis. Sci. **27**, 145-52 (1986)
17. F. C. Delori and K. P. Pflibsen, "Spectral reflectance of human ocular fundus," Appl. Opt. **28**, 1061-77 (1989)

1. Introduction

Around the world, experienced physicians are aware of the irregular reflex appearances from high-order ocular aberration, including KC, that are observed using hand-held retinoscopes [1-3]. Prior to computerized testing methods such as autorefraction, the retinoscope was the main method for objective measurement of refractive error and identification of irregular astigmatism. Although a retinoscope is a low-cost, simple optical device, the retinal reflex integrates ocular information through all optical elements similar to that of a wavefront aberrometer. Shortcomings of the current retinoscope include the broad-spectrum of the light source that integrates chromatic aberration in the measurement and the visible irradiation that stimulates pupil response and hence, in a non-mydriatic examination, reduces the examined pupillary area. Furthermore, retinoscopic observations cannot be stored in digital form for discussion and sharing. Because photorefraction (PR) shares similar optical features with retinoscopy [4, 5], it inherits the capability of detecting irregular aberration but without the shortcomings of the retinoscope. The objective of this paper is to visualize aberration from an irregular cornea using computer simulation of PR. To do so, personalized schematic eye models were constructed from the measured clinic data of five eyes with keratoconus and 8 ametropic eyes.

Detailed optical eye modeling is possible when the measured corneal topography, wavefront aberration, and biometric data are accessible [6]. These models can assist ocular surgical planning [7-9], and in designing of personalized intraocular lens, spectacles, and contact lens. [10-12]. Here, we utilize personalized modeling in computer simulations to predict clinical measurements. To validate the simulation result, the results were compared to experimental measurements of equivalent optical conditions. Validated ophthalmic simulations with personalized eye models make it possible to investigate accurately the instrument sensitivity using the clinic database without additional testing on real patients.

2. Photorefraction simulation

To investigate keratoconus detection using the PR technique, optical schematic eye models of individuals were constructed using ZemaxTM optical software (ZEMAX Development Corporation, Bellevue, WA, USA). The average optical parameters of human eyes were adopted from a wide-angle emmetropic eye model [13]. Existing clinical data including the corneal topography and refraction prescription of five eyes with keratoconus and eight ametropic eyes were used for the individual eye modeling.

Keratonconus is a corneal disease where the cornea becomes thin and cannot sustain a normal shape. The corneal surface becomes distorted and irregularly shaped, leading to a loss of best corrected vision. Retinoscopy reveals a 'scissor-reflex' in these eyes of varying degrees. Scarring, straie (or folds) of the back surface of the cornea, and bullous keratopathy (bubbles of swelling in the cornea) may occur as the disease progresses and these can also be seen in the retinal reflex. Diagnosis is typically based on the clinical picture. In mild cases, the topographical map is irregular but the patient has no other clinical signs. In moderate

#74906 - $15.00 USD Received 11 September 2006; revised 26 October 2006; accepted 30 October 2006

cases, the patient may suffer loss of best corrected vision, show more astigmatism on topography, and have a thinned cornea based on ultrasound measurement. In severe cases, the best corrected vision is severely reduced, topography is highly irregular when obtainable, and the cornea may show signs of scarring, swelling, and/or stria.

For this study, clinical measurements for five patients with mild-to-moderate keratoconus were obtained. The anterior surface of the base eye model [13] was replaced with the elevation map of corneal topography from a Humphrey Atlas system. After the corneal topography was measured and saved, the elevation files were exported using the external interface of the Humphrey MasterVue topography system. The elevation files were then used by a Matlab program to determine the missing corneal surface. The missing interior corneal surface elevation data was linear interpolated based on Delaunay triangulation techniques. The missing peripheral data was linearly extrapolated horizontally, vertically, and diagonally to neighboring nodes. The reconstructed corneal elevation results were then used by Zemax to reproduce the corneal surface for optical eye modeling. After the replacement of cornea surface, the individual model was modified to approach the refraction as found in the clinical record by manifest refraction. The aperture stop was set to 3 mm diameter (pupil about 3.4 mm) and the wavelength at 555 nm. The vitreous length was set to be a variable for iteration to produce the patients' prescribed spherical equivalent refraction (SE). Minimization of RMS wavefront error was used as the merit function in the ZEMAX optimization.

After this optimization, the models' SE were equivalent to the patients' clinical data. The five normal myopic eyes (average spherical equivalence = -5.15 diopters) had an average axial length of 26.0 mm, three normal hyperopic patients (average spherical equivalence = +1.8 diopters) had an average axial length of 23.7 mm, and the 5 KC patients (all myopic with an average spherical equivalence = -3.5 diopters) had an average axial length of 24.6 mm. The average length for emmtropic eyes is 24 mm.

Subsequent to the vitreous length procedure, the next step was to achieve the individual clinical cylinder refraction. To do this, at the aperture stop (true pupil) location was placed a 3-variable paraxial thin lens that was comprised of two cylinders (two variables) in perpendicular meridians, and the axial rotation of this paraxial lens was allowed to be the third variable. For a 3-mm aperture setting, the forward optical optimization was again performed simultaneously for the three variables and achieved the exact refraction prescription of the individual eye. Since the total higher-order aberration of the individual eye was unknown, this Gaussian thin lens compensates only the second-order defocus, including astigmatism, but does not alter the higher order contribution. After the optimizations, in all thirteen eye model cases the two perpendicular cylinders in the paraxial lens were close in magnitude with reversed sign. This ensures the average curvature of crystalline lens is the anatomical average value as in the base model. The 8 ametropic models were given 0.45 ± 0.2 diopters intraocular cylinders and the 5 KC eyes were given additional intraocular cylinders of 1.25 ± 0.64 diopters. The eight final ametropic model eyes, after prescription correction, had a total RMS wavefront error of 0.10 ± 0.02 μm. The five KC eye models, on the other hand, had after-correction RMS WF errors of 0.99 ± 0.73 μm, which were an order of magnitude larger than the reported 3rd-6th high-order RMS WF error norm of 0.08 μm at 4 mm pupil obtained from a large number of subjects [14]. The high-order aberrations in the KC models are primarily from the corneal surface. The intraocular optimization performed in this work is not intended to compensate for the cornea abnormality or to increase the ocular aberration in high order. The intraocular components in the models are assumed to be independent of the patients' cornea high-order features.

Photorefraction simulation was performed with the camera focal plane located at the plane of the anterior cornea. A shorter-than-typical working distance of 30 cm between camera and the subject was used to obtain better spatial resolution, and a larger-than-normal camera entrance pupil of 18 mm was used to provide more dynamic range of the reflex signal. At same working distance of the camera entrance pupil, thirteen 5-mm-diameter Lambertian

#74906 - $15.00 USD Received 11 September 2006; revised 26 October 2006; accepted 30 October 2006

light sources of 800nm wavelength were located coaxially and at three eccentricities of 6.5, 9.0, and 11.5 mm (measured from the center of camera pupil to the center of each of the four light source) in the 4 directions of up, down, left, and right.

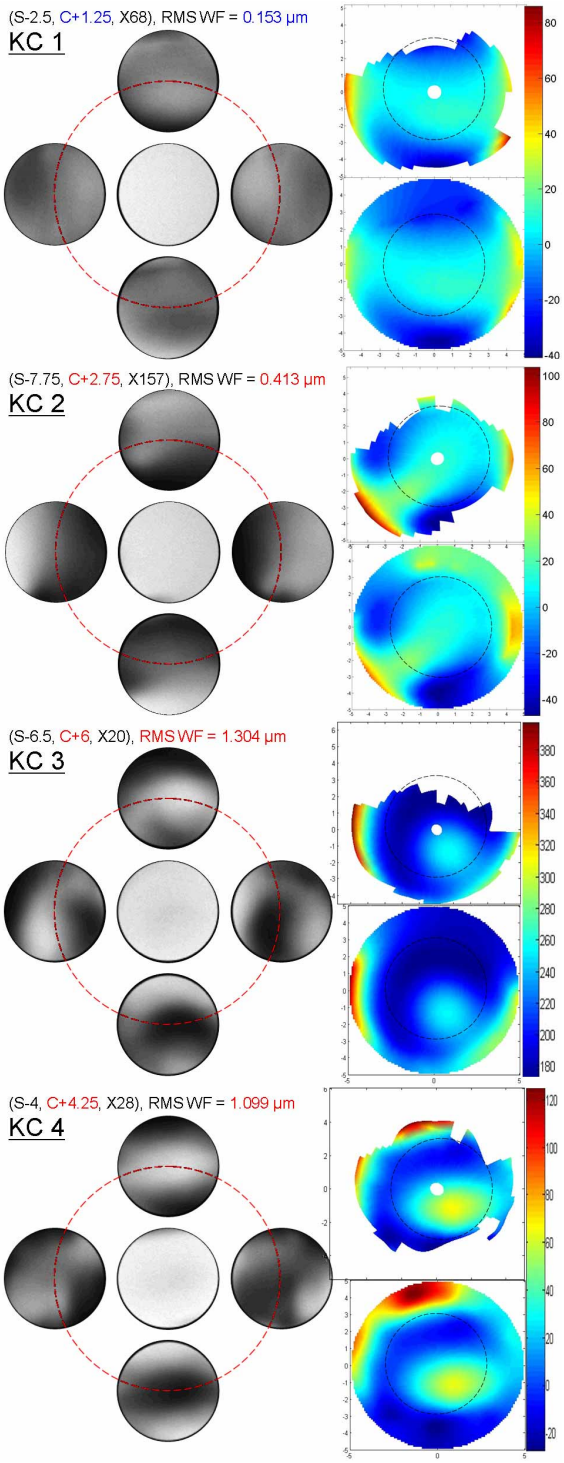

#74906 - $15.00 USD Received 11 September 2006; revised 26 October 2006; accepted 30 October 2006

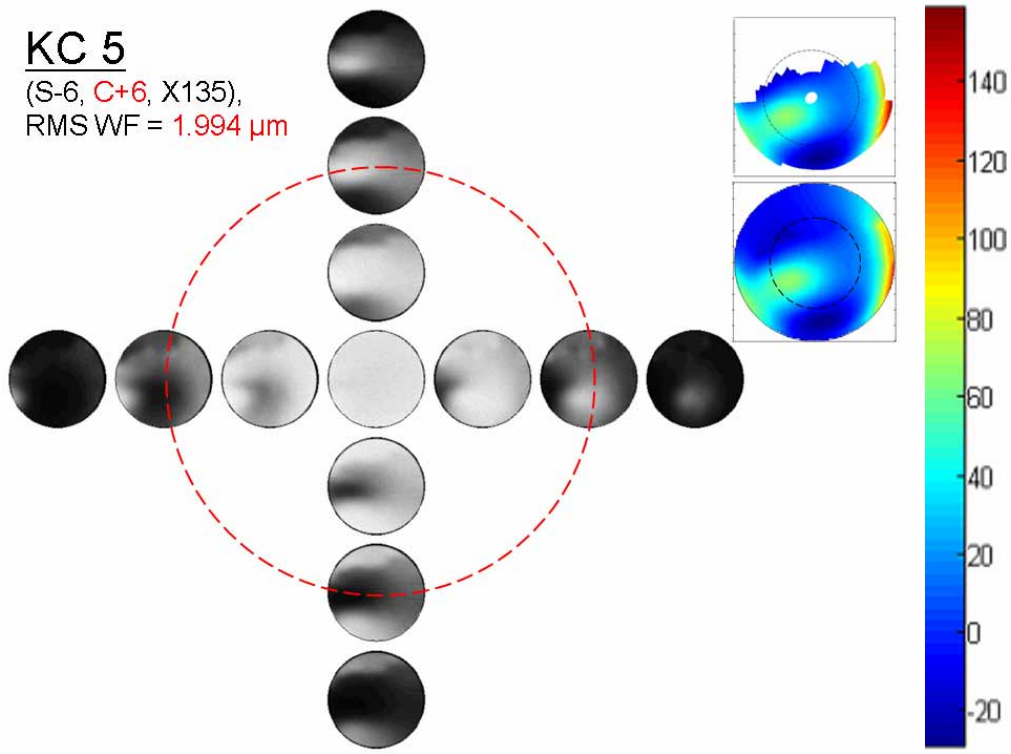

Fig. 1. PR simulation results (left) and measured and filled corneal topographies (upper and lower right) of model eyes from 5 KC patients. The lower (blue) to upper (red) scales in each color bar of the 5 KC topographies are -14 to +80 µm, -40 to 100 µm, 180 to 380 µm, -20 to 120 µm, and -20 to 140 µm respectively. KC_5 simulation was performed for eccentricities of 0 (coaxial), 6.5, 9 (knife-edge), and 11.5 mm. Camera entrance pupil is 18 mm as indicated with red dashed lines.

The 9 mm-eccentricity condition corresponds to the knife-edge PR arrangement, which is sensitive in aberration detection [15]. The subject eye was assumed to be relaxed in the simulation, and double-pass image-analysis was performed through ray tracing. Chromatic indices of all ocular elements were calculated based on the parameters given in the Navarro model [13]. Assuming natural dilation in the dark measurement environment, the pupil sizes of all eye models, except for KC_5 and MY_3, were set to be 6 mm. For comparison to the experiment data, 6.1 mm and 5.6 mm were used for KC_5 and MY_3 respectively.

Other than the larger pupil coverage and sharper intensity variation, infrared photorefraction is similar to spot retinoscopy. The photorefraction result shows that the small gazing angles and the angle (kappa) between the visual and pupillary axes cause only a slight shift in the PR reflex images. The thirteen simulation results with eyes looking straight forward are shown in Figs 1, 2, and 3. On the right side of each set of simulations in the three figures are the clinically measured and, for comparison, the computer inter- and extrapolated corneal topography. A floating best-fit sphere was subtracted from the raw elevation data to emphasize the detailed corneal structures. The circular dashed lines on the topographies indicate the reference pupil boundaries of PR calculations. Also shown on the top left of each set of results are the refraction prescription and the after-correction RMS wavefront error of the eye model.

#74906 - $15.00 USD Received 11 September 2006; revised 26 October 2006; accepted 30 October 2006

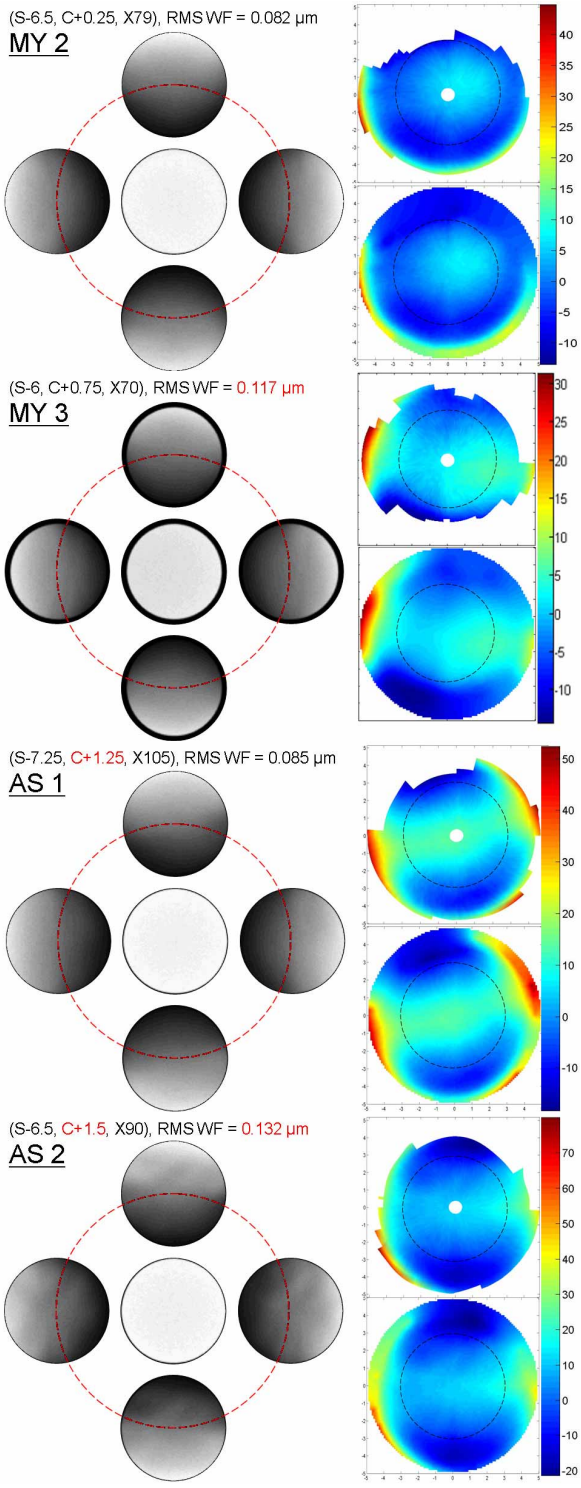

Fig. 2. Corneal topographies (right) and PR simulation results (left) of 4 myopic eyes. The lower (blue) to upper (red) scales in each color bar of the 4 myopic topographies are -10 to +40 µm, -10 to 30 µm, -10 to 50 µm, and -20 to 70 µm respectively.

#74906 - $15.00 USD Received 11 September 2006; revised 26 October 2006; accepted 30 October 2006

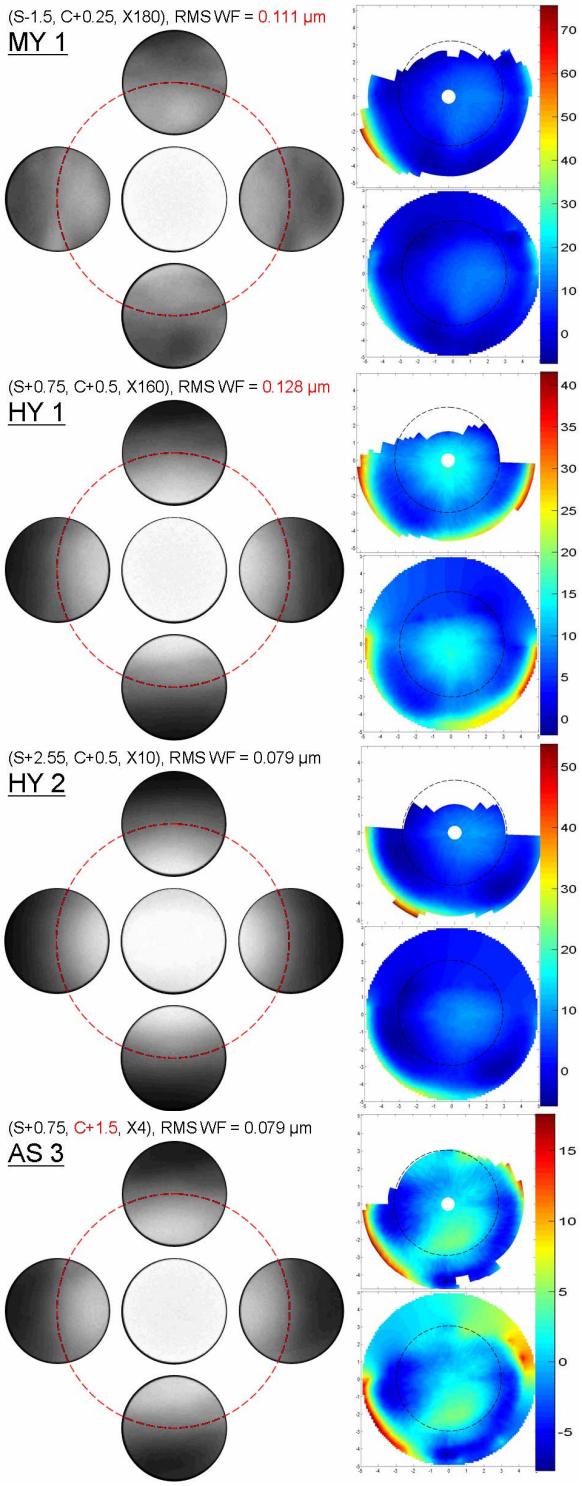

Fig. 3. Corneal topography (right) and PR simulation results of a mild myopia and 3 hyperopic eyes. The lower (blue) to upper (red) scales in each color bar of the 4 topographies are 0 to 70 µm, 0 to 40 µm, 0 to 50 µm, and -5 to 15 µm respectively.

#74906 - $15.00 USD Received 11 September 2006; revised 26 October 2006; accepted 30 October 2006

Figure 1 shows the predicted observations of the five KC eyes. These images show irregular intensity distributions across the pupil areas. The expected four knife-edge eccentric images show the most distinguished intensity variation in the reflex observation (illustrated in the KC_5 simulation). One common observation in the five KC eyes is the bright spot which appears near the cone when illumination is from the upper eccentricity of the camera. These brighter spots represent the convergent reflex distributions caused by the lower-located KC cones. When illuminated from the lower eccentric location, a shadow appears approximately at the cone location, which demonstrates the divergent reflex from the cone. Similar to the up and down illumination, the left and right PR images in the knife-edge setting also show the bright-dark reversed images. The coaxial PR images are not sensitive in detecting the irregular corneal conditions.

Among these KC cases, KC_1 has the mildest condition, where the cone is not clearly shown on topography. The protruding ridge is about 20 μm high. The corneal cylinder is 1.25 diopter, and the after-correction aberration of 0.153 μm is not significantly larger than that of typical ammetropic eyes, such as AS_2 in Fig. 2. Although the intensity contrasts in the eccentric pupil reflexes are not as crisp as other KC cases, the common KC shadow and bright spot appearance is clearly shown, and the typical PR observation of corner crescents for ammetropic eyes are not present.

For the 30 cm working distance in this simulation, the PR center of the dark zone (or the neutralization refraction) is -3.3 diopter [4, 5, 15]. Figure 2 shows simulation results of four higher myopic eyes (>3.3 diopter) with and without significant astigmatism. The retinal reflexes clearly show the bright crescent in the corresponding directions of illumination, which is a common high myopic appearance in PR measurement. Notice that the two astigmatic eyes AS_1 and AS_2 have cylinder magnitudes similar to KC_1. The topographies of these two eyes also have similar appearances of KC_1. However, the shadow and bright spot typical to KC are not observed in these two eyes. Also noticeable is the slightly rippled reflex distribution on AS_2. This is a result from the larger high-order aberration of 0.132 μm.

The simulation result of the mild myopia, MY_1 (<3.3 diopter), and the hyperopic cases, HY_1, HY_2, and AS_3, are shown in Fig. 3. Since there is neither accommodation assumed nor the compensation 3.3-diopter trial lens included in the simulation, the retinal reflex crescents of these four eyes appear in the opposite direction of the illumination as expected with typical geometric PR analysis [5]. It is also noted that the results of MY_1 exhibit a more rippled reflex due to the high-order aberrations of this eye.

3. Validation and conclusion

To validate the simulations, photorefraction measurements were performed on one KC eye (KC_5) and one myopic eye (MY_3), each of which can be described as a moderate abnormality. The experiment used five infrared 5-mm-diameter pulsed LEDs (wavelength 805±30 nm) for illumination, a pellicle beam splitter, and a digital camera with a lens entrance pupil of 18 mm. The distance from both camera entrance pupil and light sources, through the beam splitter, to the examined eyes were 30 cm. The eccentricities and positions of LEDs were the same as described in the simulation work. The eye images were acquired in the darkened laboratory so that the pupils were naturally dilated.

Figure 4 shows the measured PR images from the KC eye (KC_5) and the myopic eye (MY_3). The pupil areas in these images were cropped for presentation. The images are nearly identical to the simulated data in Figs. 1 and 2 but for the lower contrast and more details in the measured photographs. One reason for this contrast difference is the presence of multiple intraocular scattering that is not included in the optical computation. Because of the differences in melanin density in pigment epithelium, Caucasians exhibit more pronounced retinal reflex in retinoscope, ophthalmoscope, and PR measurements and common photographs than do Asians and blacks [16, 17]. Detailed differences between simulation and

#74906 - $15.00 USD Received 11 September 2006; revised 26 October 2006; accepted 30 October 2006

measurement may be attributed to intraocular factors such as the posterior cornea and the lens that are also not included in the simulation.

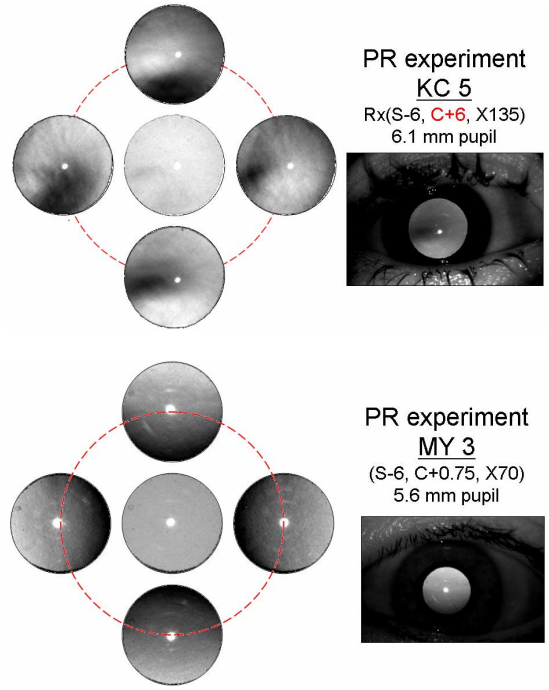

Fig. 4.. Experiment measured PR images from KC_5 (compared to simulation result in Fig. 1) and MY_3 eyes (compared to simulated images in Fig. 2). Near the center of the pupil in each image is the cornea reflection.

In this study, individualized eye models were determined from clinical measurements of refractive error and corneal topographies of subjects with mild-to-moderate degrees of myopia, hyperopia, astigmatism and KC. The 3-variable lens construct provided excellent agreement between the eye model prediction and the clinical measurements. Using the eye models, predictions were obtained for the simulated measurement results of a photorefractive instrument. These results indicated that the PR design exhibited the ability to detect such cases of KC. Moreover, because of the differences in the optical aberrations, the PR design was able to differentiate these KC measurements from not only hyperopic eyes but also from eyes characterized by degrees of simple myopia and astigmatism that are characteristic in the progression of KC. Further investigation using more mild degrees of KC patients' data that include both the anterior and posterior corneal surfaces would determine the sensitivity of this photorefractive technique in the identification of keratoconus. The enhancement of optical design to increase detection sensitivity through this technique is promising. University of Tennessee/Knoxville Institutional Review Board approval was obtained for the methods and practices of this study.

Acknowledgments

This study was partially supported by ARMY TATRC Grant W81XWH-05-1-0409.

#74906 - $15.00 USD Received 11 September 2006; revised 26 October 2006; accepted 30 October 2006